Reaction-Diffusion Network Models for Alzheimer's Disease.

MATHEMATICAL INSTITUTE, UNIVERSITY OF OXFORD

Case Study in Mathematical Modelling

Candidate number: 1077723

Date: September 11, 2024

Abstract. The current theory of neurodegenerative diseases like Alzheimer's (AD) holds that the prion-like formation and spread of pathological protein aggregates in the brain along anatomically connected networks plays a central role in cognitive decline, structural damage, and ultimately death of the affected individual. Pathologically, AD is characterised by the accumulation of toxic amyloid-beta (Aβ) and tau-protein (τP) following specific spatial progressions through the brain, and brain atrophy beyond normal ageing. This project undergoes a comprehensive exploration of AD, through the development of network reaction-diffusion models for the spread of toxic τP. We will see how even the simplest models (Fisher-KPP) can recover the shape, staging and timescales of AD's biomarker curves. We will then move to a model considering a more detailed description of protein dynamics including nucleation, aggregation, depolymerisation and clearance mechanisms, as well as clearance deterioration due to the build-up of toxic τP. Finally, we will augment this model to consider brain atrophy in the form of axonal pathway degeneration and volume loss.

1 Introduction

1.1. Prion Diseases

Proteins [1] are the base of cellular structure, metabolism, and communication. Each type of protein has a different role and, to fulfil it adequately, it must fold properly into a specific 3D structure. A healthy cell has quality-control mechanisms that ensure proteins are properly produced, folded, and eliminated. If these mechanisms are impaired it can lead to pathology.

Common disorders of this type are prion diseases [1, 2, 3, 4], where misfolded protein molecules (prions) act as corruptive seeds that aggregate and impose their anomalous structure on healthy molecules. This chain reaction of aggregation and misfolding leads to the generation of intracellular and or extracellular deposits that can cause a diverse range of pathologies.

Prion proteins are found most abundantly in the brain, which is physically and functionally organised as a network, optimised for transmitting information [3]. Unfortunately, it seems that misfolded proteins spread mainly through neuronal pathways [4] so this optimality also applies to the spread of prions. The current theory of neurodegenerative diseases like Alzheimer's (AD) holds that the prion-like formation and spread of pathological protein aggregates in the brain along anatomically connected networks plays a central role in cognitive decline, structural damage, and ultimately cause the death of the affected individual. This is known as the prion-like hypothesis [1, 2, 3, 4] .

1.2. Alzheimer's Disease (AD)

Over the past century, with an ageing world population, AD has become a priority for global neurodegenerative disease research [2, 5]. AD is the most common cause of dementia, affecting 1 in 14 people over the age of 65 and 1 in every 6 people over the age of 80 [5]. Pathologically, AD is characterised by the accumulation of toxic amyloid-beta (Aβ) and tau-protein (τP) following specific spatial progressions through the brain, and brain atrophy beyond normal ageing [1, 5, 6, 7]. However, since many cellular mechanisms are poorly understood in vivo, it is hard to establish the relative contribution of the different toxic proteins (and their interactions) to atrophy.

Aβ [1, 2, 3, 8] is a normal metabolic waste by-product of the cleavage of the Aβ precursor protein, although its physiological role remains undetermined. When it misfolds, it forms extracellular aggregates and plaques, so it mainly spreads through the extracellular matrix. Previously, the accumulation of toxic amyloid-beta (Aβ) protein was thought to be not only an early indicator of the disease but the primary driver (amyloid-beta hypothesis [2, 8]). However, experimental evidence revealing that Aβ plaques can develop over many years without associated cognitive decline, and the failure in clinical trials focused on the reduction of Aβ plaques has led to the search for other possible mechanisms [2, 8].

τP [1, 2, 3] is a cytoplasmatic protein that normally helps to stabilise microtubules. When it misfolds, it can form large disorganised neurofibrillary tangles (NFTs) which propagate intracellularly to anatomically connected sites in the network of axonal pathways. Significant evidence suggests that τP, not only contributes to the disease, but its accumulation marks the start of cognitive decline [2, 9]. Hence, attributing a more prominent role in the progression of AD to τP has become an obvious alternative to the amyloid-beta hypothesis, and its study is becoming increasingly popular.

Findings suggest that the accumulation of Aβ and τP promotes brain atrophy beyond what is associated with normal ageing. Two of the main forms it takes are progressive axonal degeneration and destruction [6], and volume loss [7, 10, 11].

1.3. This Project

This project aims to simulate the spread of toxic τP through the brain using a network reaction-diffusion model. In section 2, we will give a quick theoretical introduction to this type of model and its objectives. In section 3, we will go over the specifics of the network used. Section 4 will explore how the simplest protein kinetic model can recover the shape, pattern, and timescales of invasion of τP. Next, in section 5, we will consider a more complete model including nucleation, aggregation, depolymerisation, and clearance mechanisms, as well as clearance deterioration due to the build-up of toxic τP. We will give a complete analysis of its behaviour at the single node, network, and organ levels. Finally, in section 6, we will augment this model to consider brain atrophy in the form of axonal pathway degeneration and volume loss.

2 Theory: General Staging Problem

Consider a continuous domain B representing the brain, with boundary δB. The evolution of the concentration $p(\boldsymbol{x}, t)$ of misfolded τP can be described as the diffusion-reaction dynamical system

$$\frac{\mathrm{d}p(\boldsymbol{x},t)}{\mathrm{d}t} = \rho\nabla\cdot(\boldsymbol{K}\cdot\nabla p(\boldsymbol{x},t)) + f(t,p(\boldsymbol{x},t)), \qquad \boldsymbol{x}\in B, \tag{1a}$$

$$p(\boldsymbol{x},0) = p_0(\boldsymbol{x}), \qquad \boldsymbol{x}\in B, \tag{1b}$$

$$(\boldsymbol{K}\cdot\nabla p(\boldsymbol{x},t))\cdot\hat{\boldsymbol{n}}(\boldsymbol{x}) = 0, \qquad \boldsymbol{x}\in \delta B, \tag{1c}$$

where ρ is the effective diffusion constant, $\boldsymbol{K}$ is the diffusion tensor, f is the reaction term, $p_0(\boldsymbol{x})$ is the initial seeding, and $\hat{\boldsymbol{n}}$ is the normal to the boundary [12]. Note that (1) the first term on the right-hand side of eq. (1a) is Fick's law of diffusion, and (2) the Neumann boundary condition (eq. (1c)) enforces mass conservation in the absence of a reaction term (i.e. τP proteins can only be created or destroyed via reactions).

Now consider a brain network $G = (V, E)$, with nodes $V = \{v_i\}_{i=1}^N$ representing anatomical regions and edges $E = \{e_{ij}\}_{i,j=1}^M$ representing the connectivity between regions v_i and v_j. The evolution of concentrations $\{p_i(t)\}_{i=1}^N$ at each node from an initial seeding $p_{i,0}$ can be found discretising eqs. (1a) to (1c) as

$$\frac{\mathrm{d}p_i(t)}{\mathrm{d}t} = -\rho\sum_{j=1}^{N}\mathcal{L}_{ij}p_j(t) + f(t,p_i(t)), \qquad i = 1,2,...,N, \tag{2a}$$

$$p_i(0) = p_{i,0}, \qquad i = 1,2,...,N, \tag{2b}$$

where $\boldsymbol{\mathcal{L}}$ is the graph Laplacian [12]. To enforce an equivalent of Fick's law of diffusion (i.e. that transport is driven by a difference in concentrations), we must have

$$\boldsymbol{\mathcal{L}}\cdot\mathbf{1} = 0, \tag{3}$$

where $\mathbf{1} = (1,1,...,1)$. To enforce the Neumann boundary condition (eq. (1c)), $\boldsymbol{\mathcal{L}}$ must conserve mass. Let $\boldsymbol{p} = (p_1, p_2, ..., p_N)$ and $\boldsymbol{\nu} = (\nu_1, \nu_2, ..., \nu_N)$, where ν_i is the volume of node v_i. Then, when the reaction term in eq. (2a) is zero,

$$\frac{\mathrm{d}\boldsymbol{p}(t)}{\mathrm{d}t} = -\rho\boldsymbol{\mathcal{L}}\cdot\boldsymbol{p}(t), \tag{4}$$

and conservation of total mass M requires

$$\frac{\mathrm{d}M}{\mathrm{d}t} = \sum_{i=1}^{N} \nu_i \frac{\mathrm{d}p_i(t)}{\mathrm{d}t} \equiv \boldsymbol{\nu} \cdot \frac{\mathrm{d}\boldsymbol{p}(t)}{\mathrm{d}t} = 0. \tag{5}$$

Substituting eq. (4) into eq. (5) gives $\boldsymbol{\nu} \cdot (\boldsymbol{\mathcal{L}} \cdot \boldsymbol{p}) = 0$, which must hold for all $\boldsymbol{p}$. Hence,

$$\boldsymbol{\nu} \cdot \boldsymbol{\mathcal{L}} = 0. \tag{6}$$

As demonstrated in [12], eqs. (3) and (6) can be met choosing

$$\boldsymbol{\mathcal{L}} = \nu \boldsymbol{V}^{-1} \boldsymbol{L}, \tag{7}$$

where $\boldsymbol{V} = \mathrm{diag}(\boldsymbol{\nu})$, ν is a characteristic volume (for simplicity we take $\nu = 1\ \mu\mathrm{m}^3$, another option would be $\nu = \sum_{i=1}^{N} \nu_i$), and $\boldsymbol{L}$ is the standard graph Laplacian

$$\boldsymbol{L} = \boldsymbol{D} - \boldsymbol{W}, \tag{8}$$

where $\boldsymbol{W}$ is the weighted adjacency matrix that codifies the connectivity between the vertices of G, and $\boldsymbol{D}$ is the diagonal degree matrix defined by $D_{ii} = \sum_{j=1}^{N} W_{ij}$.

In this project, we explore how different modelling decisions — reaction terms, parameter values, etc. — modify how the disease spreads. We will identify the best choices by assessing which evolutions are closer to clinical observations. To do so, we must establish some metrics to characterise the evolution of neurodegeneration [3, 12]. First, we define a collection of disjoint subsets of V $\{\Omega_j\}_{j=1}^{J}$ representing the brain regions where τP spreads at each stage of the disease. As $p_i(t)$ evolves according to eqs. (2a) and (2b), we calculate the average concentration of misfolded τP (biomarker abnormality) at each Ω_j. We then expect the brain to get infected in an ordered sequence Ω_1, Ω_2, ..., Ω_J following the clinically observed spreading pattern.

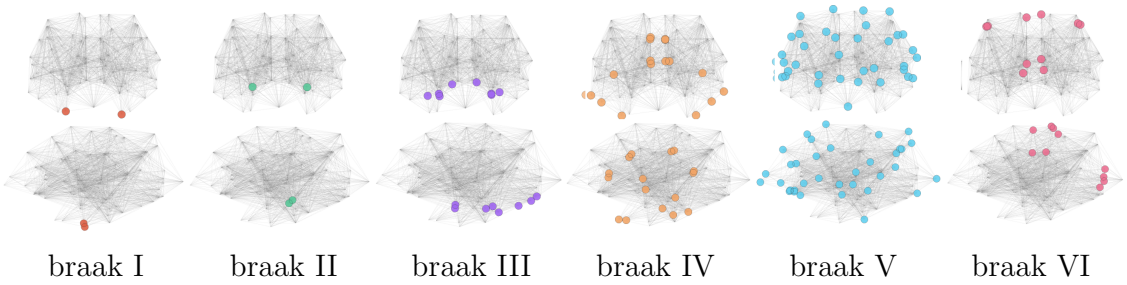

Fig. 1: Front and side view of the braak regions $\{\Omega_i\}_{i=1}^{6}$ on the connectome.

3 Methods

In this project we consider a network G of $N = 83$ nodes and $M = 1654$ edges built from the data generated by the Human Connectome Project (HCP) [13]. The number of edges per node varies between a minimum of 12 at the frontal pole and a maximum of 67 at the thalamus. Each edge e_{ij} has an associated number of fibres, n_{ij}, and fibre length, l_{ij}. Following [3], we choose a "ballistic weighting"

$$W_{ij} = \frac{n_{ij}}{l_{ij}}. \tag{9}$$

which is then normalised so that $\boldsymbol{W}$ has no units.

We also define a preferred activation sequence. As shown in fig. 1, we define six regions of the brain, $\{\Omega_i\}_{i=1}^{6}$, called "braaks", which have been observed to be infected by toxic τP in stages [1, 2, 3, 12, 14]. Starting at the entorhinal cortex (braak I), τP spreads to the rest of the medial temporal lobe, namely the hippocampus, essential for short-term memory (braak II). After the rest of the temporal lobe — crucial to language — is infected (braak III), τP spreads to other zones of the limbic system — responsible for emotion, behaviour, and long-term memory — and the insula (braak IV). Finally, τP extends widely into other neocortical association areas and the brainstem — responsible for vital functions like breathing and sleeping — (braak V) and then to the primary sensory and motor cortices (braak VI). Hence, at the beginning of the simulations, we seed toxic τP at braak I (Ω_1) with

$$p_i(0) = \begin{cases} 1/20, & i|v_i \in \Omega_1, \\ 0, & i|v_i \notin \Omega_1. \end{cases} \tag{10}$$

The simulations in future sections use a common set of model parameters (Table 1).

Parameter	Description	Value
ρ	effective diffusion constant	0.01 yr^{-1}
α	conversion rate from healthy to misfolded state	2.10 yr^{-1}
λ_{crit}	clearance value above which no aggregates are formed	0.72 yr^{-1}
λ_∞	minimum clearance value	0.01 yr^{-1}
β	node vulnerability	1.00 yr^{-1}
a	rate of volume loss due to aging	0.005 yr^{-1}
γ	rate of volume loss due to AD	0.005 yr^{-1}

Table 1: Description and numerical values of the parameters used.

4 Fisher-KPP Model

4.1. Model

We start by considering the simplest mathematical description of protein misfolding.

$$\hat{p} \xrightarrow{\alpha} p \tag{11}$$

That is, healthy proteins $\hat{p}$ misfold to the toxic state p with a local conversion rate α. Adding these reaction kinetics to eq. (1a) gives the Fisher-Kolmogorov-Petrovsky-Piskunov (Fisher-KPP) model [3, 12]

$$\frac{\mathrm{d}p(\boldsymbol{x},t)}{\mathrm{d}t} = \rho\nabla\cdot(\boldsymbol{K}\cdot\nabla p(\boldsymbol{x},t)) + \alpha p(\boldsymbol{x},t)(1-p(\boldsymbol{x},t)), \tag{12}$$

where $p \in [0,1]$ and has no units. This system has an unstable fixed point $p^* = 0$ that corresponds to a completely healthy state, and a stable fixed point $p^* = 1$ that corresponds to a completely infected state. Moreover, it has two asymptotic regimes:

$$\begin{aligned} \text{Diffusion-dominated} \quad & \alpha \ll \rho, \\ \text{Growth-dominated} \quad & \rho \ll \alpha. \end{aligned}$$

We can discretise eq. (12) to the form of eq. (2a) giving

$$\frac{\mathrm{d}p_i(t)}{\mathrm{d}t} = -\rho\sum_{j=1}^{N}\mathcal{L}_{ij}p_j(t) + \alpha p_i(t)(1-p_i(t)), \qquad i = 1,2,...,N. \tag{13}$$

4.2. Results and Discussion

4.2.1 Diffusion- and Growth-Dominated Regimes

Figure 2 shows the two asymptotic regimes of Fisher-KPP, both displaying a smooth sigmoidal shape, in agreement with clinical biomarker models of neurodegeneration [3]. However, the diffusion-dominated regime does not display the expected spreading pattern discussed in section 3, where the braaks are infected in stages. On the other hand, the growth-dominated regime agrees perfectly with it. Hence, from now on, we will only work within the growth-dominated regime setting $\rho = 0.01$ yr^{-1} as recorded in table 1.

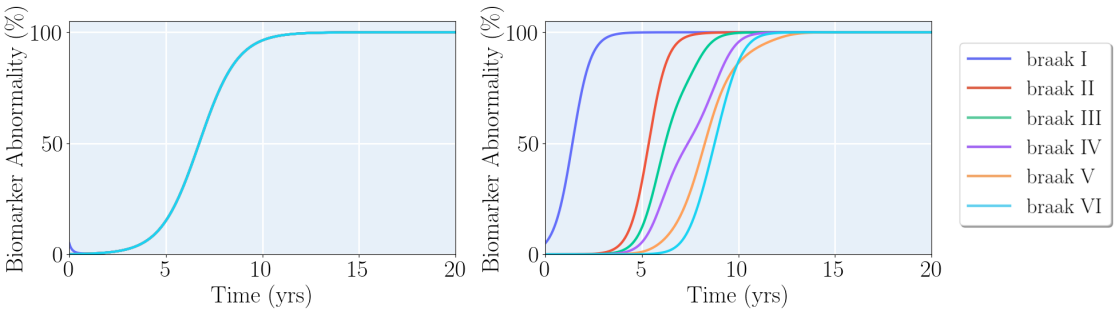

Fig. 2: Asymptotic regimes of the Fisher-KPP model. Equation (13) was integrated using explicit Euler. α was chosen as defined in table 1 and ρ was set to 100 yr^{-1} for the diffusion-dominated regime (left) and 0.01 yr^{-1} for the growth-dominated regime (right). The initial conditions were set to eq. (10).

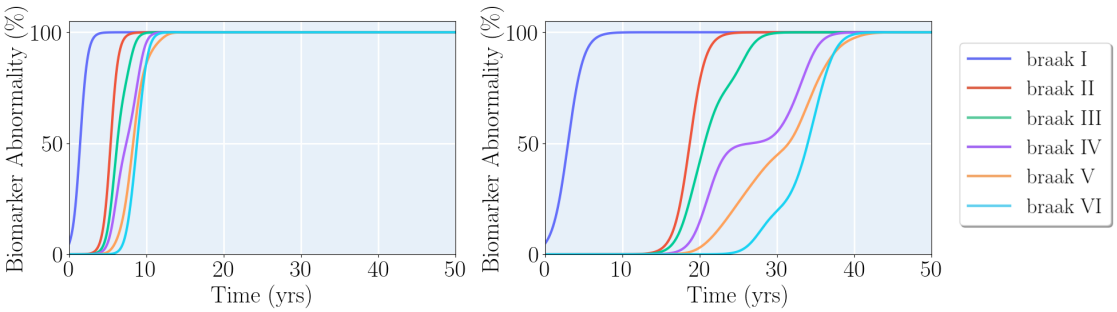

Fig. 3: Effect of taking volume into account in the Fisher-KPP model. Equation (13) was integrated using explicit Euler. α and ρ were chosen as defined in table 1 and $\boldsymbol{\nu}$ was set to $\mathbf{1}$ μm^3 for the left plot and to the values generated by HCP [13] for the right plot. The initial conditions were set to eq. (10).

4.2.2 Volume

In the previous sections, we assumed all nodes had the same volume (i.e. $\boldsymbol{\nu} = \mathbf{1}$ μm^3). Figure 3 shows how the biomarker curves change when differences in the volume of each brain region are accounted for. The lines curve horizontally (especially braak IV) because now each region's volume is larger, taking longer to infect it. This gives a more accurate timescale for the evolution of the disease in each region with respect to the others. Hence, from now on we will take into account the different volumes.

4.3. Conclusion

Equation (13) is a good starting point for modelling the spread of toxic τP through the brain. It can recreate the shape, staging, and timescale of invasion of τP. Still, it is greatly limited by the crudeness of the kinetics it considers (eq. (11)). The main consequence of this oversimplification is that there is only one stable fixed point at $p^* = 1$, so intermediate equilibrium states are not captured. As soon as a misfolded protein appears ($p > 0$), the brain will become completely infected. In reality, low levels of toxic τP can be present in a healthy brain without leading to pathology [4, 8].

5 Protein Kinetics and Clearance

5.1. Model

The aggregation of τP into NFTs is more complicated than eq. (11). Smoluchowski models capture its dynamics more accurately by thinking of healthy τP as monomers (■) which group into larger toxic oligomers (□□$\cdots$□), namely the NFTs. The total concentration of monomers is $\hat{p}$, and the total concentration of oligomers of all sizes is p. Then, we have the following processes

monomer production: ∅ → ■ (14a)

primary nucleation: ■ + ■ → □□ (14b)

secondary nucleation: ■ + ■ + □□$\cdots$□ → □□ + □□$\cdots$□ (14c)

aggregation: ■ + □□$\cdots$□ → □□$\cdots$□□ (14d)

depolimerisation: □□$\cdots$□□ → □□$\cdots$□ + ■ (14e)

Moreover, cells also have clearance mechanisms that remove unnecessary healthy and pathological species, limiting the formation of aggregates and preventing, or at least delaying, the disease.

monomer clearance: ■ → ∅, (15a)

oligomer clearance: □$\cdots$□□ → ∅ (15b)

Thompson et al. [8] demonstrated that assuming the clearance rate λ is size independent (i.e. monomers and oligomers of any size are eliminated at the same rate)

and close to a critical value λ_{crit}, the dynamics at the local level takes the form of a transcritical bifurcation

$$\frac{\mathrm{d}p(t)}{\mathrm{d}t} = -(\lambda - \lambda_{\text{crit}})p(t) - \alpha p(t)^2, \tag{16}$$

where $p \notin [0, 1]$, but it still has no units. Unlike for the Fisher-KPP, the healthy state ($p^* = 0$) is stable if $\lambda > \lambda_{\text{crit}}$, solving the issue of having only one stable critical point corresponding to the diseased state. However, it loses stability as $\lambda < \lambda_{\text{crit}}$ and the toxic state becomes the only stable fixed point. We can now take eq. (16) to represent the local reaction term of eq. (2a).

Finally, it is also known that the build-up of toxic τP can lead to the impairment of clearance mechanisms. To take this into account, we augment the system to include a deterioration of clearance at each node λ_i towards a minimum value λ_∞ with a first-order rate law [4],

$$\frac{\mathrm{d}p_i(t)}{\mathrm{d}t} = -\rho \sum_{j=1}^{N} \mathcal{L}_{ij} p_j(t) - (\lambda_i(t) - \lambda_{\text{crit}})p_i(t) - \alpha p_i(t)^2, \qquad i = 1, 2, ..., N, \tag{17a}$$

$$\frac{\mathrm{d}\lambda_i(t)}{\mathrm{d}t} = -\beta p_i(t)(\lambda_i(t) - \lambda_\infty), \qquad i = 1, 2, ..., N, \tag{17b}$$

where β is the node vulnerability.

5.2. Results and Discussion

5.2.1 Single Node Dynamics

If the initial conditions are the same at each node (i.e. $p_{i,0} = p_0$, $\lambda_{i,0} = \lambda_0$) the system eqs. (17a) and (17b) is equivalent to that of a single node

$$\frac{\mathrm{d}p(t)}{\mathrm{d}t} = -(\lambda(t) - \lambda_{\text{crit}})p(t) - \alpha p(t)^2, \tag{18a}$$

$$\frac{\mathrm{d}\lambda(t)}{\mathrm{d}t} = -\beta p(t)(\lambda(t) - \lambda_\infty). \tag{18b}$$

This system has two fixed points $(p^*, \lambda^*) = ((\lambda_{\text{crit}} - \lambda_\infty)/\alpha, \lambda_\infty), (0, \lambda)$ which, respectively, are unconditionally stable and conditionally stable (only for $\lambda > \lambda_{\text{crit}}$). These fixed points correspond to a diseased node when $((\lambda_{\text{crit}} - \lambda_\infty)/\alpha, \lambda_\infty)$, a susceptible node when $(0, \lambda)$ and $\lambda < \lambda_{\text{crit}}$, and a healthy node when $(0, \lambda)$ and $\lambda > \lambda_{\text{crit}}$.

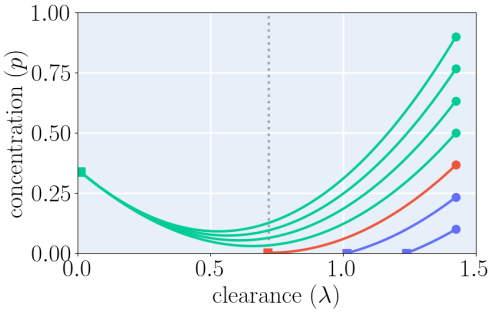

Fig. 4: Response of a healthy node ($p = 0$, $\lambda > \lambda_{\text{crit}}$), to an increase Δp in τP concentration. Equations (18a) and (18b) were integrated using explicit Euler. The dotted grey line marks λ_{crit}. Blue lines represent $\Delta p < p_{\text{crit}}$, green lines represent $\Delta p > p_{\text{crit}}$, and the red line represents $\Delta p = p_{\text{crit}}$. The parameters used in these simulations are given in table 1.

Susceptible and healthy nodes differ in their reaction to an increase Δp in toxic τP concentration. On one hand, susceptible nodes will invariantly evolve to the diseased state. Meanwhile, for healthy nodes the clearance will be reduced but, depending on the toxic load Δp, they will evolve to a healthy ($\Delta p < p_{\text{crit}}$), susceptible ($\Delta p = p_{\text{crit}}$), or diseased ($\Delta p > p_{\text{crit}}$) state. This is shown in fig. 4 and an analytical expression for p_{crit} is derived in [4]. Similarly, diseased nodes react to a decrease $-\Delta p$ in toxic τP by increasing p back to the stable state.

Hence, looking at eq. (17a), we see that, at the network level, as soon as there is one diseased node present, the whole brain is fated to become infected. That is because toxic τP seeds will be incubated at this node and diffused to its healthy neighbours until their clearance is reduced below λ_{crit} and they transition to a diseased state. Then, a brain is healthy if all its nodes are healthy, susceptible as soon as one node is susceptible, and diseased as soon as one node is diseased.

5.2.2 Network Dynamics

In this section, we move from a single node to a star graph and explore the effect of diffusivity and network connectivity on the critical toxic seeding value p_{crit} of the central node (i.e. Δp needed to reach the state $(0, \lambda_{\text{crit}})$). To vary the diffusivity of the system we modify ρ and to vary the network connectivity we change the number of neighbours.

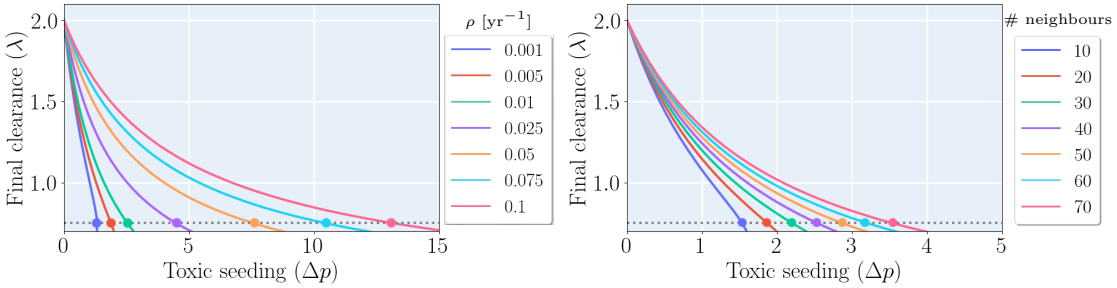

Fig. 5: Effect of diffusivity and network-connectivity on the critical toxic seeding p_{crit}. Equations (17a) and (17b) were integrated using explicit Euler. Dots represent p_{crit} of each trajectory. The systems considered were a node with 40 neighbours and a varying ρ (left) and a node with a varying number of neighbours and a fixed $\rho = 0.01$ yr^{-1}(right). The rest of the parameters used in these simulations are given in table 1. The initial conditions were set to be $p_i(0) = 0$ and $\lambda_i(0) = 2.0$ yr^{-1} in all nodes except the central node for which $p_i(0) = \Delta p$.

Figure 4 (b)-(c) shows that, as diffusivity and connectivity increase, the critical toxic seeding is larger. These results suggest that enhanced diffusivity and network connectivity may protect the brain from disease by distributing the burden of eliminating high quantities of toxic τP between neighbours [4].

5.2.3 Disease Dynamics

Finally, we will explore the effect of clearance on the disease progression at the organ level. For these simulations, we initially set clearance to be $\lambda_i(t) = \lambda_0$ at all nodes. Figure 6 shows that, as λ_0 increases, the disease is delayed and eventually prevented when $\lambda_{i,0} > \lambda_{\text{crit}}$. At $\lambda_0 = \lambda_{\text{crit}}$, only braak I evolves to the fully diseased state in the span of 100 years. The other brain regions get infected but at a much slower timescale which is imperceptible in these plots.

5.3. Conclusion

This model is a good improvement from the FKPP for it is not only able to recover the biomarker curves of a diseased brain, but it is also able to capture intermediate healthy and susceptible equilibrium states. However, this model is limited as it does not account for atrophy beyond the deterioration of clearance.

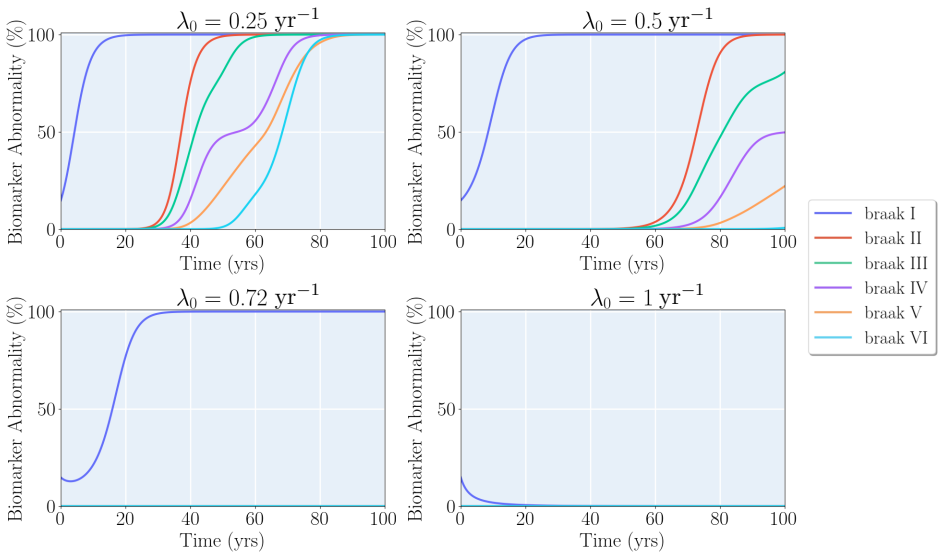

Fig. 6: Effect of clearance on disease progression. Equations (17a) and (17b) were integrated using explicit Euler. The parameters used in these simulations are given in table 1. For these values concentration of toxic τP saturates at $p^* = (\lambda_{\mathrm{crit}} - \lambda_\infty)/\alpha \simeq 0.338$. The initial conditions were set to eq. (10) and $\lambda_i(0) = \lambda_0$.

6 Brain Atrophy

6.1. Model

We will now augment the model developed in the previous section to account for brain atrophy in the form of deterioration of the axonal pathways and volume loss. As a first step towards this goal, we augment the system of equations eqs. (17a) and (17b) by adding a first-order equation for damage evolution

$$\frac{\mathrm{d}q_i(t)}{\mathrm{d}t} = \beta p_i(t)(1 - q_i(t)), \qquad i = 1, 2, ..., N, \tag{19a}$$

where damage is a dimensionless quantity $q \in [0, 1]$. We take the same node vulnerability β as for clearance for there is no reason to believe it would be different. This damage can then be used to modify the connectivity between nodes as follows

$$\tilde{\mathcal{L}}_{ij}(t) = \mathcal{L}_{ij} \max\left\{\frac{e^{2\kappa - q_i(t) - q_j(t)} - 1}{e^{2\kappa} - 1}, 0\right\}, \tag{19b}$$

where $\kappa \in [0, 1]$ is a constant that must be specified. When $q_i + q_j \geq 2\kappa$ the conexion between regions i and j is completelly broken (i.e. $\tilde{\mathcal{L}}_{ij} = 0$). Hence, κ effectively sets the cut-off damage above which axonal pathways do not allow transport of toxic τP.

Next, we further extend our model by adding an equation for volume loss

$$\frac{\mathrm{d}v_i(t)}{\mathrm{d}t} = -(a + \gamma p_i(t))v_i(t), \qquad i = 1, 2, ..., N, \tag{19c}$$

where a is the rate of volume loss due to normal ageing, and γ is the rate of volume loss due to the build-up of toxic τP. Note that this makes eq. (7) time dependent. The brain undergoes a normal volume loss of 5% per decade past the age of 40 [10]. Hence we take $a = 0.005$ yr^{-1} and choose to set γ to the same value. To take this variation of volume into account in eq. (17a), from the definition of concentration $p_i \propto v_i^{-1}$, we must add an extra $-\frac{p_i(t)}{v_i(t)}\frac{\mathrm{d}v_i}{\mathrm{d}t}$.

Taking the deterioration of axonal pathways and volume loss into account,

$$\frac{\mathrm{d}p_i(t)}{\mathrm{d}t} = -\rho \sum_{j=1}^{N} \tilde{\mathcal{L}}_{ij}(t)p_j(t) - (\lambda_i - \lambda_{\mathrm{crit}})p_i(t) - \alpha p_i(t)^2 + (a + \gamma p_i(t))p_i(t), \qquad i = 1, 2, ..., N. \tag{19d}$$

Note that this addition changes the fixed points and now, in a similar way to what was discussed in section 5.2.1, we have $(p^*, \lambda^*) = ((\lambda_{\mathrm{crit}} - \lambda_\infty + a)/(\alpha - \gamma), \lambda_\infty), (0, \lambda)$. Altogether, our model consists of eqs. (17b) and (19a) to (19d).

6.2. Results and Discussion

6.2.1 Deterioration of Axonal Pathways

We start by considering atrophy as the deterioration of the axonal pathways solely ($a = \gamma = 0$ yr^{-1}). Figure 7 shows how, as toxic τP accumulates, the entries of the laplacian decrease, thus decreasing the diffusivity and connectivity of the network, and — in line with what was demonstrated in section 5.2.2 — delaying the spread of the disease. As κ decreases, entries tend to zero faster and the disease spreads slower. Therefore, the deterioration of axonal pathways can delay the progression of AD in terms of the accumulation of toxic τP. However, it is positively correlated with other aspects of AD-like cognitive impairment [6].

6.2.2 Loss of Volume

Now, we consider atrophy as the loss of volume solely ($q_i(t) = 0$). Figure 3 shows how, as toxic τP accumulates, the volume of all regions of the brain decreases, thus

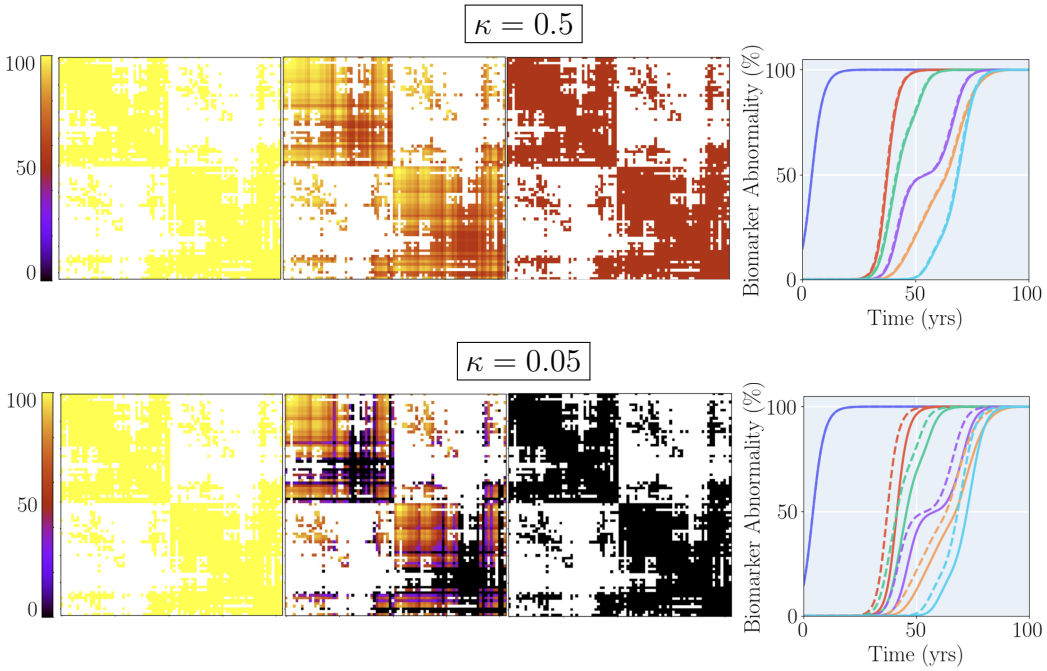

Fig. 7: Deterioration of axonal pathways as the disease evolves. Equations (17b) and (19a) to (19d) were integrated using explicit Euler. Plots show the percentage of the original laplacian entries left at three different times and the biomarker curves with damage (solid lines) and without damage ($q_i(t) = 0$, dashed lines). a and γ were set to zero and the rest of the parameters used in these simulations are given in table 1. The initial conditions were set to eq. (10) and $\lambda_i(0) = 0.25$ yr^{-1}.

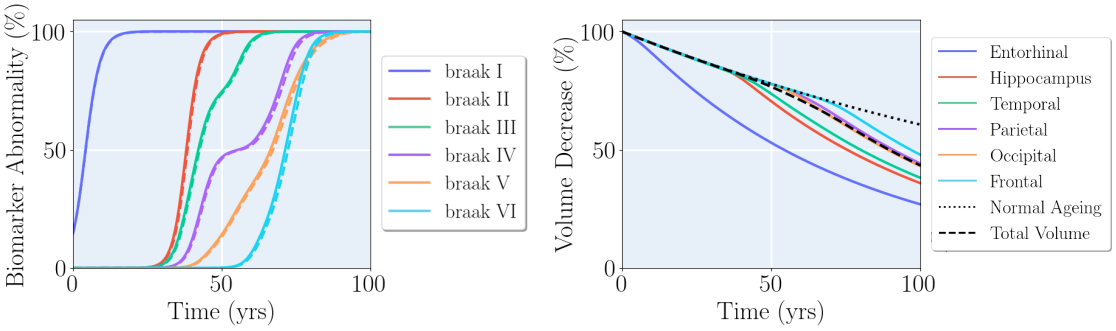

Fig. 8: Volume loss as the disease evolves. Equations (17b) and (19a) to (19d) were integrated using explicit Euler. Plots show the biomarker curves with ($a = \gamma = 0.005$ yr^{-1}, solid lines) and without volume loss ($a = \gamma = 0$ yr^{-1}, dashed lines). The rest of the parameters used in these simulations are given in table 1. The initial conditions were set to eq. (10) and $\lambda_i(0) = 0.25$ yr^{-1}.

increasing the concentration p at all nodes and speeding up the spread of the disease. Moreover, our model can recover [11]'s observations, where the entorhinal cortex and the hippocampus are the first areas affected by atrophy.

Note that volume can also be used as a reliable biomarker of AD progression. Unlike the concentration of τP, which no current technology can directly quantify non-invasively in humans, volume loss can be measured via imaging. Hence, we have developed a way in which theoretical model results can be compared to in-vivo data.

6.3. Conclusion

Our final model is a very complete description of the spread of AD which (1) recovers the clinically observed biomarker curves for both the concentration of τP and volume loss, (2) captures intermediate healthy and susceptible equilibrium states, and (3) considers brain atrophy in terms of clearance, axonal pathways, and volume.

However, there is still room for improvement. For instance, this model does not capture the effects of the accumulation of Aβ nor protein-protein interactions between Aβ and τP. There is increasing evidence [2] that these interactions play a crucial role in AD and future work should be aimed at expanding models with protein-protein interactions (e.g. [2]'s heterodimer model) to account for brain atrophy in the form of impairment of clearance, deterioration of axonal pathways and volume loss.

7 Final Conclusion

In this project, we have undergone a comprehensive exploration of Alzheimer's Disease through the development of network reaction-diffusion models. Using the Fisher-KPP model as an entry point, we saw how even the simplest models can recover the shape, staging and timescales of AD's biomarker curves. We then moved to a more complete description of protein dynamics which included nucleation, aggregation, depolymerisation and clearance mechanisms, as well as clearance deterioration due to the build-up of toxic τP. We gave an in-depth analysis of its behaviour at the single node, network, and organ levels. Finally, we augmented this model to consider brain atrophy and explored how axonal pathway degeneration and volume loss impact the evolution of Alzheimer's Disease. Future work should be aimed at extending in a similar fashion models with protein-protein interactions.

References

[1] M. Jucker and L. C. Walker. "Self-propagation of pathogenic protein aggregates in neurodegenerative diseases". *Nature* **501**.7465 (2013), pp. 45–51.

[2] T. B. Thompson et al. "Protein-protein interactions in neurodegenerative diseases: A conspiracy theory". *PLoS computational biology* **16**.10 (2020), e1008267.

[3] S. Fornari et al. "Prion-like spreading of Alzheimer's disease within the brain's connectome". *Journal of the Royal Society Interface* **16**.159 (2019), p. 20190356.

[4] G. S. Brennan et al. "The role of clearance in neurodegenerative diseases". *SIAM Journal on Applied Mathematics* (2023), S172–S198.

[5] NHS Inform. *Alzheimer's Disease*. Available at https://www.nhsinform.scot/illnesses-and-conditions/brain-nerves-and-spinal-cord/alzheimers-disease/ (2005/06/12). NHS, 2024.

[6] N. Salvadores, C. Gerónimo-Olvera, and F. A. Court. "Axonal degeneration in AD: the contribution of Aβ and tau". *Frontiers in Aging Neuroscience* **12** (2020), p. 581767.

[7] Y. Blinkouskaya and J. Weickenmeier. "Brain shape changes associated with cerebral atrophy in healthy aging and Alzheimer's disease". *Frontiers in Mechanical Engineering* **7** (2021), p. 705653.

[8] T. B. Thompson et al. "The role of clearance mechanisms in the kinetics of pathological protein aggregation involved in neurodegenerative diseases". *The Journal of chemical physics* **154**.12 (2021).

[9] C. R. Jack et al. "Tracking pathophysiological processes in Alzheimer's disease: an updated hypothetical model of dynamic biomarkers". *The lancet neurology* **12**.2 (2013), pp. 207–216.

[10] M. M. Esiri. "Ageing and the brain". *The Journal of Pathology: A Journal of the Pathological Society of Great Britain and Ireland* **211**.2 (2007), pp. 181–187.

[11] R. I. Scahill et al. "Mapping the evolution of regional atrophy in Alzheimer's disease: unbiased analysis of fluid-registered serial MRI". *Proceedings of the National Academy of Sciences* **99**.7 (2002), pp. 4703–4707.

[12] P. Putra et al. "Braiding Braak and Braak: Staging patterns and model selection in network neurodegeneration". *Network Neuroscience* **5**.4 (2021), pp. 929–956.

[13] D. Marcus et al. “Informatics and Data Mining Tools and Strategies for the Human Connectome Project”. *Frontiers in Neuroinformatics* **5** (2011).

[14] J. Weickenmeier et al. “A physics-based model explains the prion-like features of neurodegeneration in Alzheimer’s disease, Parkinson’s disease, and amyotrophic lateral sclerosis”. *Journal of the Mechanics and Physics of Solids* **124** (2019), pp. 264–281.